Modeling of a Multitube High-Temperature Solar Thermochemical Reactor for Hydrogen Production

S. Haussener
Department of Mechanical and Process Engineering,
ETH Zurich,
8092 Zurich, Switzerland

D. Hirsch

C. Perkins

A. Weimer

Department of Chemical Engineering,
University of Colorado,
Boulder, CO 80309-0424

A. Lewandowski
National Renewable Energy Laboratory,
1617 Cole Boulevard,
Golden, CO 80401-3393

A. Steinfeld
Department of Mechanical and Process Engineering,
ETH Zurich,
8092 Zurich, Switzerland;
Solar Technology Laboratory,
Paul Scherrer Institute,
5232 Villigen, Switzerland

A solar reactor consisting of a cavity-receiver containing an array of tubular absorbers is considered for performing the ZnO-dissociation as part of a two-step H_2O-splitting thermochemical cycle using concentrated solar energy. The continuity, momentum, and energy governing equations that couple the rate of heat transfer to the Arrhenius-type reaction kinetics are formulated for an absorbing-emitting-scattering particulate media and numerically solved using a computational fluid dynamics code. Parametric simulations were carried out to examine the influence of the solar flux concentration ratio (3000–6000 suns), number of tubes (1–10), ZnO mass flow rate (2–20 g/min per tube), and ZnO particle size (0.06–1 μm) on the reactor's performance. The reaction extent reaches completion within 1 s residence time at above 2000 K, yielding a solar-to-chemical energy conversion efficiency of up to 29%. [DOI: 10.1115/1.3097280]

1 Introduction

H_2O-splitting thermochemical cycles are being considered for solar hydrogen production via redox reactions involving, e.g., ZnO, MnO_2, and mixed ferrite oxides [1]. In an endothermic solar step, the metal oxide is thermally dissociated using high-temperature solar process heat. In an exothermic nonsolar step, the reduced metal or lower-valence metal oxide is reacted with H_2O to generate H_2, and the original metal oxide that is recycled. Solar reactors concepts for reducing metal oxides can be classified into those based on the direct solar irradiation through transparent windows [2,3] and those based on the indirect irradiation through opaque reactor walls [4–6]. The dissociation of ZnO has been experimentally demonstrated with both reactor concepts [2,4]. This paper deals with the redesign of a solar reactor based on the indirect irradiation concept using an opaque tube (or array of tubes) as the absorber [4]. In the single-tube configuration, a large portion of the solar power input (~40%) is lost by reradiation. A reactor model is developed for the purpose of optimizing the design for maximum solar-to-chemical energy conversion efficiency.

1.1 Reactor Design and Modeling

1.1.1 Reactor Configuration. The improved reactor design addresses the reradiation problem by enclosing the absorber tube with a cavity containing a small aperture for the access of concentrated sunlight. A compound parabolic concentrator (CPC) is incorporated into the aperture to further increase the solar flux concentration ratio C. The inner cavity walls reflect diffusely or specularly. An array of multiple tubes is considered, as shown schematically in Fig. 1. To reduce computing time, a large number of 2D simulations and a smaller set of selected 3D simulations are performed. The 2D geometry is obtained by cutting a horizontal slice in the x-y-plane through the middle of the reactor.

1.1.2 Governing Equations. The continuity, momentum, and energy conservation equations are given by

$$\frac{\partial \rho}{\partial t} + \nabla \cdot (\rho \bar{u}) = S_m \tag{1}$$

$$\frac{\partial}{\partial t}(\rho \bar{u}) + \nabla \cdot (\rho \bar{u}\bar{u}) = -\nabla p + \nabla \cdot (\mu \nabla \bar{u}) \tag{2}$$

$$\frac{\partial}{\partial t}(\rho h - p) + \nabla \cdot (\bar{u}(\rho h)) = \nabla \cdot (k \nabla T) + S_h \tag{3}$$

In solid regions, Eq. (3) becomes

$$\frac{\partial}{\partial t}(\rho h) = \nabla \cdot (k \nabla T) \tag{4}$$

The ZnO particle suspension is modeled as a semitransparent continuum. The equation of radiative transfer for an absorbing, emitting, and scattering medium is given by

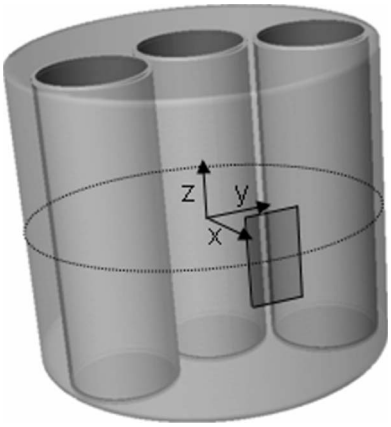

Fig. 1 Solar reactor configuration consisting of a cylindrical cavity containing an array of absorber tubes. The shadowed rectangle indicates the aperture. The dashed line indicates the *x-y*-plane used for the 2D clip.

Contributed by the Solar Energy Engineering Division of ASME for publication in the JOURNAL OF SOLAR ENERGY ENGINEERING. Manuscript received August 8, 2007; final manuscript received November 18, 2008; published online March 25, 2009. Review conducted by Gilles Flamant. Paper presented at the 2007 ASME Solar Energy Division and Advanced Energy Systems Division Conference (ES2007), Long Beach, CA, June 27–29, 2007.

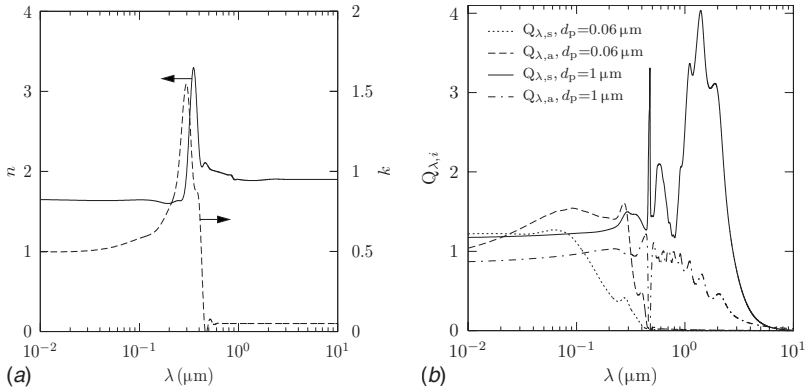

Fig. 2 (*a*) Real and imaginary part, *n* and κ, of the refractive index of ZnO. (*b*) Scattering and absorption efficiencies, $Q_{\lambda s}$ and $Q_{\lambda a}$, for 1 μm and 0.06 μm diameter ZnO particles.

Table 1 Factor definition for the first and second two-level fractional factorial analyses

	First design		Second design	
Factor	High level	Low level	High level	Low level
d_p	0.06 μm	1.00 μm	0.06 μm	0.53 μm
cavity	Diffuse	Specular	Diffuse	Specular
C	6000 suns.	3000 suns	6000 suns	4500 suns
$\dot{m}_{ZnO}$	10 g/min/tube	2 g/min/tube	10 g/min/tube	6 g/min/tube
Window aspect ratio (height:width)	3:1	0.75:1	3:1	0.75:1
r_c	0.14 m	0.1 m	0.14 m	0.12 m
N_{tubes}	5	3	5	4
r_h/r_c	0.6	1.0	0.6	0.8

$$\frac{\partial I(\vec{r},\vec{s})}{\partial s} + (a+\sigma_s)I(\vec{r},\vec{s}) = an^2 I_{\text{blackbody}}(\vec{r}) + \frac{\sigma_s}{4\pi}\int_0^{4\pi} I(\vec{r},\vec{s}')\Phi(\vec{r},\vec{s}\cdot\vec{s}')d\Omega' \quad (5)$$

Equation (5) is solved within two wavelength bands: 0–1.5 μm and 1.5–∞ μm. The solar spectrum is approximated by a 5800 K blackbody, with 90% of the emissive power in the first band. Elastic and independent scattering is assumed [7]. Mie theory is applied using the BHMIE algorithm written by Bohren and Huffman [8] implemented in MATLAB. The complex refractive index of ZnO is shown in Fig. 2(*a*) [9,10]. The absorption and scattering efficiencies for ZnO particles 1 μm and 0.06 μm in diameter are plotted in Fig. 2(*b*).

1.1.3 Reaction Kinetics. Assuming an ideal plug-flow reactor and first-order reaction [11], the reaction extent is given by

$$X = 1 - e^{-k_r\tau} \quad (6)$$

where the rate constant obeys the Arrhenius law, $k_r = k_0 e^{-E_A/RT}$, with an activation energy E_A of 356 kJ/mol and a frequency factor k_0 of 4×10^9 s^{-1} [4].

1.1.4 Numerical Algorithm. Computational fluid dynamics (CFD) is performed with FLUENT Version 6.3.21 beta, using GAMBIT Version 2.3.16 as preprocessor [12]. The discrete ordinates (DO) radiation model [13] is applied to solve Eq. (5) for a finite number of discrete angles, each associated with a vector direction $\vec{s}$ fixed in the Cartesian system [12]. Each octant of the angular space 4π at any spatial location is discretized into $N_\theta\times N_\phi$ solid control angles. $4N_\theta\times N_\phi$ and $8N_\theta\times N_\phi$ directions are solved in 2D and 3D, respectively. The governing equations are discretized and solved sequentially on the individual control volumes of the meshed geometry by the finite-volume technique with a second-order upwind scheme (Green–Gauss node-based gradient option and algebraic multigrid method). A fixed V-cycle is applied for pressure and a flexible cycle is applied for the transport equations. Convergence runs for temperature and energy balance leads to a scaled residual target for the DO intensity equation of 10^{-10}.

1.1.5 Boundary Conditions. Incoming solar radiation at the exit of the CPC is assumed diffuse and uniformly distributed. The absorption coefficient of quartz window is equal to 1 m^{-1} and 4 m^{-1} for the first and second bands, respectively. For the case of a diffusely-reflecting cavity wall, $\varepsilon=0.8$ for both bands, and the insulation is modeled with a thickness of 5 cm, outer boundary at 300 K, and thermal conductivity of 0.3 W/(m K) (typical for ZrO_2 or Al_2O_3-based ceramic insulation). For the case of a specularly-reflecting adiabatic cavity wall, $\varepsilon=0.4$ and 0.02 for the first and second bands, respectively. The absorber tubes are assumed to be made of SiC, 0.2 m in height, and approach a blackbody behavior. The input solar power is set to 6.6 kW and 8 kW for the 2D and 3D simulations, respectively, which correspond to a mean solar concentration ratio of 3000 suns[1]. For the 2D simulations, a sink-term equation is introduced

$$Q_{\text{sink}} = \dot{m}_{\text{Ar}}\cdot c_{p,\text{Ar}}\cdot(T-T_{\text{initial}}) + \dot{m}_{\text{Zn}}\cdot c_{p,\text{Zn}}\cdot(T-T_{\text{initial}}) + X\cdot\Delta H_{\text{react}}\cdot\dot{m}_{\text{ZnO}} \quad (7)$$

where the first two terms denote the sensible heat necessary to heat Ar and ZnO flows from the initial temperature (assumed 500

[1]1 sun corresponds to a solar radiative flux of 1 kW/m^2.

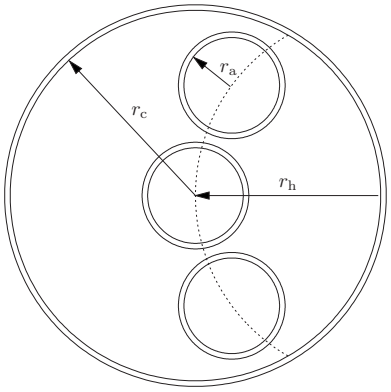

Fig. 3 Fractional factorial design parameters: cavity radius r_c, absorber tube radius r_a, and help circle radius r_h

K) to the absorber tube temperature, and the third term denotes the enthalpy change of the chemical reaction.

1.1.6 Energy Conversion Efficiencies. The absorption efficiency and the solar-to-chemical energy conversion efficiency are defined as

$$\eta_{\text{absorption}} = \frac{Q_{\text{sink}}}{Q_{\text{solar}}} \tag{8}$$

$$\eta_{\text{solar-to-chemical}} = \frac{X \cdot \Delta H_{\text{react}} \cdot \dot{m}_{\text{ZnO}}}{Q_{\text{solar}}} \tag{9}$$

1.2 Numerical Results. Two two-level fractional factorial analyses of resolution 4 [14] are applied with the baseline parameters listed in Table 1 and indicated in Fig. 3. The tubes are positioned on a "help" circle of radius r_h. The absorber tube radius r_a varies between 0.0194 m and 0.0429 m for three tubes and between 0.0105 m and 0.0246 m for five tubes. The temperature field is shown in Fig. 4 and reveals a maximum temperature gradient of 200 K in the absorber tubes for a solar flux concentration ratio of 4500 suns.

Pareto charts on $\eta_{\text{solar-to-chemical}}$ (in percent) and on the average T_{absorber} (in kelvin) are shown in Figs. 5(*a*) and 5(*b*), respectively. The most significant factor is the ZnO mass flow rate. Higher $\dot{m}_{\text{ZnO}}$ leads to higher $\eta_{\text{solar-to-chemical}}$, but lower X and T_{absorber}. In contrast, higher X can be achieved—besides a lower $\dot{m}_{\text{ZnO}}$—with a specularly-reflective cavity wall, lower N_{tubes}, and higher C. A diffusely-reflecting cavity wall promotes a more uniform temperature profile around the absorber tube and in the cavity, while decreasing the ratio of window-to-cavity area results in higher absorber temperatures. A second-order $2k'$ factorial model of the spherical central composite design (CCD) is applied, using MINITAB (Version 14.1) with $k'=3$. Figure 6 shows the contour plots of $\eta_{\text{solar-to-chemical}}$ as a function of C, $\dot{m}_{\text{ZnO}}$, and N_{tubes}. As expected, $\eta_{\text{solar-to-chemical}}$ increases with C. The combination of N_{tubes} and $\dot{m}_{\text{ZnO}}$ per tube indicates an optimum for maximum $\eta_{\text{solar-to-chemical}}$. For $Q_{\text{solar}}=8$ kW, $r_a=0.02$ m, and $N_{\text{tubes}}=6$, $\dot{m}_{\text{ZnO}}$ is optimal at 42 g/min, yielding $\eta_{\text{solar-to-chemical}}=29\%$. Table 2 lists the results of the full factorial design analysis for three tubes (runs 1–16) and for seven tubes (runs 17–24) with different absorber area per length, A_0. Higher C and $\dot{m}_{\text{ZnO}}$ lead to higher $\eta_{\text{absorption}}$, while higher C and N_{tubes} lead to higher $\eta_{\text{solar-to-chemical}}$. Since more tubes imply smaller diameters, the temperature gradient in the tube decreases (at constant total $\dot{m}_{\text{ZnO}}$) and the average fluid temperature increases, resulting in a higher reaction extent.

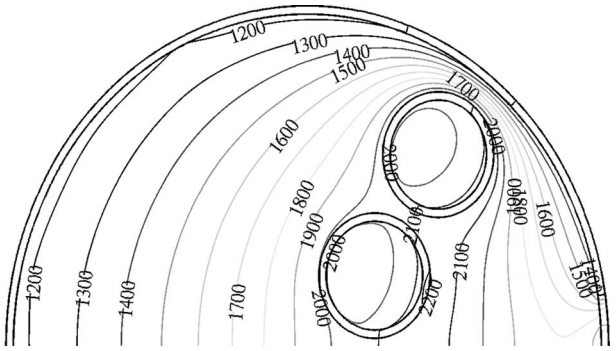

Fig. 4 Temperature field (in kelvin) for a specularly-reflecting cavity with four absorber tubes. Baseline parameters: C =4500 suns, r_c=0.12 m, r_a=0.0227 m, r_h=0.096 m, and $\dot{m}_{\text{ZnO}}$ =6 g/min per tube.

2 Summary and Conclusions

CFD was applied to solve the continuity, momentum, and energy conservation equations formulated for a cavity-receiver containing an array of tubular reactors for the thermal dissociation of

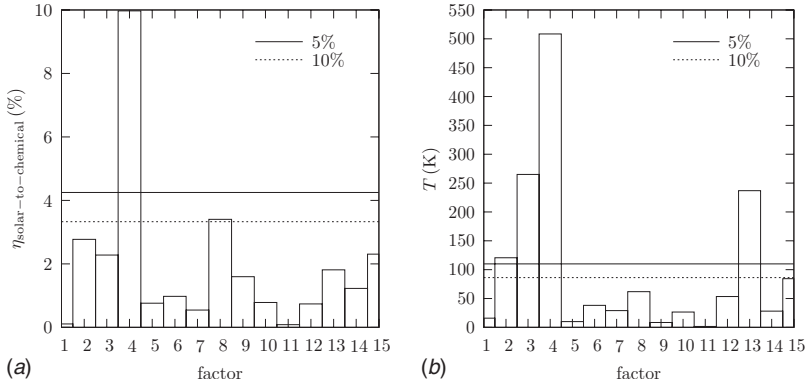

Fig. 5 Pareto charts on (*a*) the solar-to-chemical energy conversion efficiency (in percent) and (*b*) the average absorber tube temperature (in kelvin). The two lines indicate the boundary for 5% and 10% probability of type 1 error. Factor numbers denote (1) d_p, (2) specularly/diffusely-reflecting cavity, (3) C, (4) $\dot{m}_{\text{ZnO}}$, (5) window aspect ratio, (6) r_c, (7) r_h, (8) N_{tubes}, (9) d_p^* specularly/diffusely-reflecting cavity, (10) $d_p^* C$, (11) $d_p^* \dot{m}_{\text{ZnO}}$, (12) d_p^* window aspect ratio, (13) $d_p^* r_c$, (14) $d_p^* r_h$, and (15) $d_p^* N_{\text{tubes}}$.

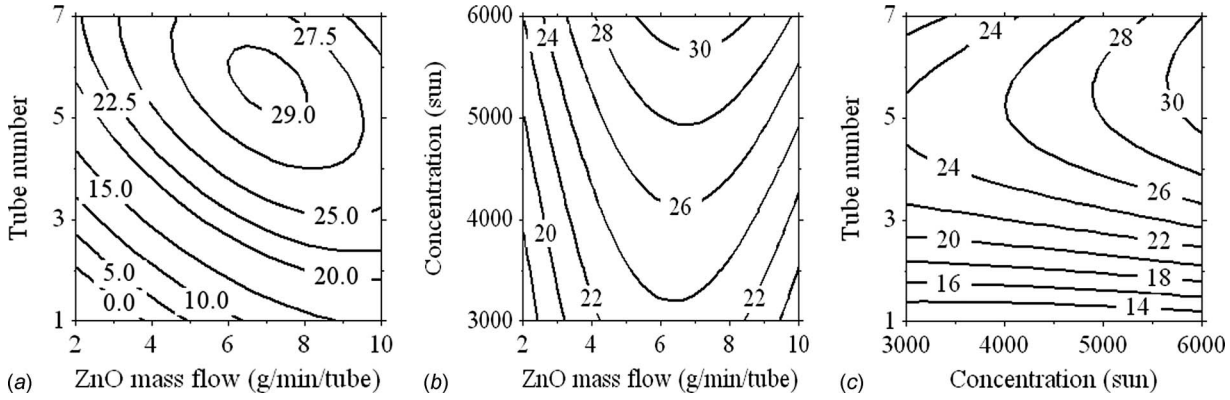

Fig. 6 Contour plots for $\eta_{\text{solar-to-chemical}}$ (%) as a function of (*a*) $\dot{m}_{\text{ZnO}}$ and N_{tubes}, (*b*) $\dot{m}_{\text{ZnO}}$ and C, (*c*) C and N_{tubes}. In each plot, the high level of the third parameter is kept constant (C=5392 suns, N_{tubes}=6, and $\dot{m}_{\text{ZnO}}$=7.16 g/min/tube).

Table 2 Parameters and results of the two (runs 1–16 and 17–24) full factorial design analyses

Run	C (suns)	$\dot{m}_{\text{ZnO}}$ (g/min/tube)	N_{tubes}	r_a (m)	A_0 (m)	$\eta_{\text{absorption}}$ (%)	$\eta_{\text{solar-to-chemical}}$ (%)	X	T_{absorber} (K)
1	3000	4	3	0.048	0.9	25.25	13.99	0.952	2042
2	3000	8	3	0.048	0.9	29.38	17.27	0.58	1925
3	3000	9.3	3	0.048	0.9	29.95	17.48	0.502	1906
4	3000	18.7	3	0.048	0.9	31.9	16.62	0.241	1826
5	6000	4	3	0.048	0.9	28.03	14.66	1	2340
6	6000	8	3	0.048	0.9	35.99	23.42	0.788	1979
7	6000	9.3	3	0.048	0.9	36.51	23.62	0.679	1950
8	6000	18.7	3	0.048	0.9	37.85	22.24	0.322	1852
9	3000	4	3	0.027	0.5	19.3	14.59	0.998	2117
10	3000	8	3	0.027	0.5	26.03	20.1	0.673	1947
11	3000	9.3	3	0.027	0.5	26.67	20.36	0.583	1925
12	3000	18.7	3	0.027	0.5	29.14	19.46	0.277	1840
13	6000	4	3	0.027	0.5	20.21	14.65	1	2474
14	6000	8	3	0.027	0.5	32.95	26.71	0.898	2019
15	6000	9.3	3	0.027	0.5	33.81	27.16	0.777	1977
16	6000	18.7	3	0.027	0.5	35.64	25.75	0.364	1866
17	3000	4	7	0.02	0.9	29.01	22.13	0.641	1939
18	3000	8	7	0.02	0.9	31.55	21.39	0.308	1852
19	6000	4	7	0.02	0.9	35.79	28.64	0.83	1992
20	6000	8	7	0.02	0.9	37.7	27.34	0.393	1876
21	3000	4	7	0.011	0.5	26.66	22.07	0.635	1938
22	3000	8	7	0.011	0.5	29.33	21.33	0.305	1849
23	6000	4	7	0.011	0.5	33.53	28.75	0.825	2094
24	6000	8	7	0.011	0.5	35.74	27.58	0.391	1873

ZnO. The solar flux concentration ratio, ZnO mass flow rate, number of tubes, and their dimensions are the most important parameters affecting the reaction extent, absorber temperature, absorption efficiency, and solar-to-chemical energy conversion efficiency. High solar flux concentration ratios lead to superior performance. For a solar input power of 8 kW, absorber radius of 0.02 m, and a six tube configuration, a total $\dot{m}_{\text{ZnO}}$ of 42 g/min is optimal, yielding a maximum $\eta_{\text{solar-to-chemical}}$ of 29%. For a constant total $\dot{m}_{\text{ZnO}}$, larger r_a results in higher temperature gradients and, consequently, a reduced T_{absorber} and lower reaction extent. For a selected absorber area, A_0, more and smaller tubes are preferred.

Acknowledgment

The authors thank the U.S. Department of Energy Hydrogen Program (Grant No. DE-PS36-03G093007), the Swiss Federal Office of Energy (Grant No. BFE-102420), and the Swiss National Science Foundation (Grant No. SNF-200021-115888) for financially supporting this work.

Nomenclature

A_0 = area per length (m)
a = absorption coefficient (m^{-1})
C = solar flux concentration ratio
c_p = specific heat capacity (J kg^{-1} K^{-1})
d_p = particle diameter (m)
E_A = activation energy (J mol^{-1})
h = specific enthalpy (J kg^{-1})
I = intensity (W m^{-2} sr^{-1})
k = thermal conductivity (W m^{-1} K^{-1})
k_r = rate constant (s^{-1})
k_0 = frequency factor (s^{-1})
$\dot{m}$ = mass flow rate (kg s^{-1})
N_{tubes} = number of absorber tubes
N_θ = number of polar angles
N_ϕ = number of azimuthal angles
n = real part of refractive index
p = pressure (Pa)
$Q_{\lambda,a}$ = absorption efficiency

$Q_{\lambda,s}$ = scattering efficiency
Q_{sink} = sink term (W)
Q_{solar} = solar power input (W)
R = universal gas constant (8.314 J K^{-1} mol^{-1})
$\bar{r}$ = position vector (m)
r_a = absorber tube radius (m)
r_c = cavity radius (m)
r_h = help circle radius (m)
s = path length (m)
$\bar{s}$ = direction vector (m)
$\bar{s}'$ = scattering direction vector (m)
S_m = mass source term (kg m^{-3} s^{-1})
S_h = volumetric heat source term (W m^{-3})
T = temperature (K)
$T_{absorber}$ = absorber temperature (K)
$T_{initial}$ = initial temperature (K)
t = time (s)
$\bar{u}$ = velocity vector (m s^{-1})
X = reaction extent
ΔH_{react} = reaction enthalpy change (J kg^{-1})
ε = emissivity
η = efficiency
θ = polar angle (rad)
κ = imaginary part of the refractive index
λ = wavelength (m)
μ = dynamic viscosity (kg m^{-1} s^{-1})
ρ = density (kg m^{-3})
σ = Stefan-Boltzmann constant (5.672×10^{-8} W m^{-2} K^{-4})
σ_s = scattering coefficient (m^{-1})
τ = residence time (s)
Φ = scattering phase function
Ω' = solid angle (rad)

References

[1] Steinfeld, A., 2005, "Solar Thermochemical Production of Hydrogen—A Review," Sol. Energy, **78**, pp. 603–615.
[2] Schunk, L., Haeberling, P., Wepf, S., Wuillemin, D., Meier, A., and Steinfeld, A., 2008, "A Solar Receiver-Reactor for the Thermal Dissociation of Zinc Oxide," ASME J. Sol. Energy Eng., **130**, p. 021009.
[3] Roeb, M., Sattler, C., Klüser, R., Monnerie, N., de Oliveira, L., Konstandopoulos, A. G., Agrafiotis, C., Zaspalis, V. T., Nalbandian, L., Steele, A., and Stobbe, P., 2006, "Solar Hydrogen Production by a Two-Step Cycle Based on Mixed Iron Oxides," ASME J. Sol. Energy Eng., **128**, pp. 125–133.
[4] Perkins, C. M., 2006, "Solar Thermal Decomposition of ZnO in Aerosol Flow to Facilitate Renewable Production of Hydrogen," Ph.D. thesis, University of Colorado, Boulder, CO.
[5] Melchior, T., and Steinfeld, A., 2008, "Radiative Transfer Within a Cylindrical Cavity With Diffusely/Specularly Reflecting Inner Walls Containing an Array of Tubular Absorbers," ASME J. Sol. Energy Eng., **130**(2), p. 021013.
[6] Epstein, M., Olalde, G., Santén, S., Steinfeld, A., and Wieckert, C., 2008, "Towards the Industrial Solar Carbothermic Production of Zinc," ASME J. Sol. Energy Eng., **130**(1), p. 014505.
[7] Siegel, R., and Howell, J., 2002, *Thermal Radiation Heat Transfer*, Taylor & Francis Inc., New York, Chap. 11.
[8] Bohren, C. F., and Huffman, D. R., 1983, *Absorption and Scattering of Light by Small Particles*, Wiley, New York.
[9] Srikant, V., and Clarke, D. R., 1998, "On the Optical Band Gap of Zinc Oxide," J. Appl. Phys., **83**, pp. 5447–5451.
[10] Al-Hilli, S. M., and Willander, M., 2006, "Optical Properties of Zinc Oxide Nano-Particles Embedded in Dielectric Medium for UV Region: Numerical Simulation," J. Nanopart. Res., **8**, pp. 79–97.
[11] Levenspiel, O., 1999, *Chemical Reaction Engineering*, Wiley, New York, Chap. 5.
[12] 2006, Fluent Reference Manual 6.3.21 Beta, Fluent, Inc.
[13] Murthy, J. Y., and Mathur, S. R., 1998, "Finite Volume Method for Radiative Heat Transfer Using Unstructured Meshes," J. Thermophys. Heat Transfer, **12**(3), pp. 313–321.
[14] Montgomery, D. C., 2005, *Design and Analysis of Experiments*, Wiley, New York.